Nuclear Physics B174 (1980) 300–316

HADRONIC ENERGY FLOW IN LEPTOPRODUCTION: A TEST OF QCD

E.K. MANESIS

Ioannina University, Greece

N.A. PAPADOPOULOS[1]

Institut für Theoretische Physik, Eidgenössische Techn. Hochschule, Zürich, Switzerland

Received 1 April 1980

Polar and azimuthal distributions of hadronic energy released in deep inelastic neutrino and antineutrino production are calculated to the first order of perturbative quantum chromodynamics. The energy dependence of these distributions perpendicular to the current momentum is studied in the rest system of the hadrons. Leptonic momenta are completely integrated out in the final state to facilitate comparison with present data. The non-perturbative background is estimated to lie below the QCD result at large polar angles, even at presently available neutrino energies. The different energy dependence of perturbative and non-perturbative results suggests a model-independent way to decide QCD dominance.

1. Introduction

After the first positive indications from total cross section data, evidence in favor of QCD is growing on the basis of less "global" measures [1]. Since no direct proof is presently expected for the existence of quarks and gluons due to confinement, one has to be satisfied with the observation of hadronic jets presumably generated from them. Indeed, several observables have been proposed to measure the jet-like configuration of an event associated with large momentum transfer(s) such as, the Sterman-Weinberg formula [2], spherocity [3], thrust [4, 5], angular energy patterns [6–8] or inclusive distributions [7, 9]. These quantities are infrared (IR) finite at least by construction, and therefore calculable in perturbative QCD. Arguments are presented to all orders in some instances [10, 7], that the logarithmic singularities in these observables are cancelled or factored away into the distribution functions. These ideas have been applied up to now mainly to $e^+e^- \to$hadrons, which is a single scaled (Q^2) reaction without initial state complications. In deep inelastic

[1] Address after April 1st 1980: Institut für Physik, Johannes Gutenberg-Universität, 6500 Mainz, Germany.

scattering, however, the situation is more delicate. This is so not only because an additional scale (W, the invariant mass of the hadrons) is introduced, or q^2 dependent distribution functions are needed: non-perturbative hadronization corrections to some variables (thrust and spherocity) seem to dominate perturbative QCD, at presently available energies [1, 11]. Undoubtedly, *other* IR finite measures should be employed here, before deep inelastic processes are excluded as a good place to test QCD in detail even at the SPS.

This attitude is pursued in this work. An observable simpler than thrust or spherocity is selected, the angular energy distribution or "antenna pattern" which is heuristically proved to be IR finite to all orders in perturbation theory [7]. Specifically, this variable is IR safe with respect to final-state logarithms because of the energy weighting and the inclusive summation involved. It is further free of initial-state logarithms in the sense that they are absorbable into parton distribution functions. Infrared safety of this observable has been explicitly demonstrated in ref. [12].

In this paper we study in detail the polar [13] and azimuthal distributions of hadronic energy flow in deep inelastic neutrino and antineutrino production to the first order of QCD. We examine further the energy and Q^2 dependence of these distributions. The momentum of the final-state lepton is integrated out completely to facilitate direct comparison with expected data [14]. The results are reasonably stable with respect to model-dependent variations of the structure functions, especially for neutrino initialized reactions.

The non-perturbative (NP) background is approximated by the hadronized contribution of the zero-order (two-jet) result, assuming a gaussian angular profile [5, 11] for the hadronic fragments in the current fragmentation region. The characteristic angular breadth of this distribution is calculated for three different parametrizations of the common fragmentation function. The induced variation in the NP estimate, as well as its average magnitude, diminish with incident energy. Comparison with the first-order result indicates that QCD dominates over the NP background at large angles, even for the leptonic beams available today. This should be contrasted with analogous QCD calculations of thrust and spherocity distributions [11], where similar estimates of the NP background lead to the opposite comparative conclusion.

Definitions, kinematics and part of the final formulae for the energy cross sections are given in sect. 2. In sect. 3 the NP contribution is estimated in the framework of a gaussian-type angular fragmentation model. The numerical results for the "antenna patterns" defined in sect. 2 are presented and discussed in sect. 4. At $\vartheta = 90°$ the energy dependence of the QCD results turn out to be quite different than the NP backgrounds. This seems to offer another possibility to decide the question of perturbative over NP dominance, and to extract $\alpha_s(Q^2)$. Finally, two appendices contain calculational details and the structure function parametrizations used in the text.

2. Energy cross sections

In the framework of QCD, energy cross sections were initially introduced in $e^+e^- \to$ hadrons to describe angular distributions of the hadronic energy [6]. A straightforward generalization of these "antenna patterns" to leptoproduction processes,

$$\text{lepton}\,(k_1) + \text{target}\,(P) \to \text{lepton}\,(k_2) + \text{hadrons}, \tag{1}$$

is given by [13]

$$\frac{d\Sigma}{d\Omega} = \sum_{i,n,j} \int dQ^2 \frac{d\xi}{4p_i\cdot k_1} \frac{d\tilde{\Sigma}_{ij}^{(n)}}{dQ^2\, d\xi\, d\Omega} f_i(\xi, Q^2),$$

$$\frac{d\tilde{\Sigma}_{ij}^{(n)}}{dQ^2\, d\xi\, d\Omega} = \int \frac{d^3k_2}{2k_2^0(2\pi)^3} p_j^0 \frac{|\boldsymbol{p}_j|^2 d|\boldsymbol{p}_j|}{2p_j^0(2\pi)^3} \prod_{\substack{k=1\\k\neq j}}^{n} \frac{d^3p_k}{2p_k^0(2\pi)^3}$$

$$\times (2\pi)^4 \delta^4\left(q + p_i - \sum_1^n p_j\right) \delta(q^2 + Q^2)\, \delta\left(\xi - \frac{p_i\cdot q}{p\cdot q}\right) |T_i^{(n)}|^2. \tag{2}$$

Each hadron is assumed to deposit energy essentially along the jet axis of its parent parton ($d\Omega$ hadron $\simeq d\Omega$ jet axis) in the subprocess $q + p_i \to p_1 + \cdots + p_n$, $q = k_1 - k_2$. Except for the energy factor p_j^0, eq. (2) is nothing more than the usual expression for the differential cross section $d\sigma/d\Omega$. $f_i(\xi, Q^2)$ is the distribution function, inside the target, of the initial parton with momentum fraction ξ as "measured" by the weak current probe at $-Q^2$. Primordial transverse momenta of quarks or gluons inside a nucleon and Fermi motion inside the target are neglected. An estimate of the angular spread of hadrons inside a final-state jet is given in sect. 3.

The observable defined above is infrared finite and well behaved, provided the angular range of energy detection does not include the current-target direction, and therefore it is calculable in perturbative QCD [7]. A part of the diagrams relevant to the lowest-order calculation in perturbative theory, $n = 2$ in eq. (2), are shown in fig. 1. The complete set includes $\{(i,j)\} = \{(q, q), (q, g), (\bar{q}, \bar{q}), (\bar{q}, g), (g, q), (g, \bar{q})\}$.

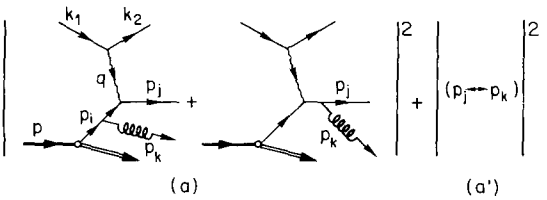

Fig. 1. Contribution of the lowest-order QCD diagrams to the antenna patterns in leptoproduction. p_i denotes the momentum of the initial quark, while p_j represents the final parton "observed" at an angle ϑ with respect to $\boldsymbol{q}$, in the $\boldsymbol{P} + \boldsymbol{q} = 0$ frame. We have similar graphs for initial antiquark or gluon.

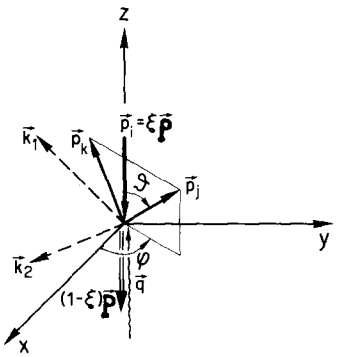

Fig. 2. The rest system of the final hadrons: $\boldsymbol{p}_j + \boldsymbol{p}_k + (1-\xi)\boldsymbol{P} = 0$. The lepton momenta lie on the xz plane. The "hadronic" plane is defined by $\{\varphi = \cos^{-1}(\hat{x}\cdot\hat{p}_j)$: fixed, $\hat{p}_{j\perp}\cdot\hat{q} = 0\}$.

The geometry of reaction (1) is defined in fig. 2 in the target-current c.m. frame, $\boldsymbol{P} + \boldsymbol{q} = \boldsymbol{0}$, to the first order in α_s.

As a specific example we consider the neutrino (antineutrino) induced production process,

$$\nu(\bar{\nu}) + \text{isoscalar target} \rightarrow \mu^- (\mu^+) + \text{hadrons}, \tag{3}$$

and neglect the strangeness-changing or charm excitation components of the weak charged current.

The polar-angle distribution of total hadronic energy, $W = \sqrt{(P+q)^2}$, carried off by non-"spectator" constituents of the target is calculated to the specified order. "Spectator" constituents are assumed to hadronize essentially along the target-fragmentation direction ($\vartheta \simeq \pi$). A small angular cutoff around the z-axis of fig. 2 is necessary to guarantee IR finiteness and calculability for all the "antenna patterns" studied here. The usual tree-graph technique delivers for massless quarks and gluons

$$\sum' |T_q^{(\nu)}|^2 = 2^7\pi\alpha_s G^2 Q^2 \frac{(k_1\cdot p_i)^2 + (k_2\cdot p_j)^2}{(p_i\cdot p_k)(p_j\cdot p_k)} \frac{4}{3},$$

$$\sum' |T_{\bar{q}}^{(\nu)}|^2 = 2^7\pi\alpha_s G^2 Q^2 \frac{(k_1\cdot p_j)^2 + (k_2\cdot p_i)^2}{(p_i\cdot p_k)(p_j\cdot p_k)} \frac{4}{3},$$

$$\sum' |T_g^{(\nu)}|^2 = 2^7\pi\alpha_s G^2 Q^2 \frac{(k_1\cdot p_k)^2 + (k_2\cdot p_j)^2}{(p_i\cdot p_k)(p_j\cdot p_i)} \frac{4}{8}. \tag{4}$$

Σ' denotes the operation ($\text{sum}_f \otimes \text{average}_i$) over all the discrete partonic degrees of freedom. The color factors are shown explicitly at the end. $G = 1.02\cdot 10^{-5} m_p^{-2}$ is

the Fermi constant. Since muon masses are also neglected, $\Sigma'|T_q^{(\bar{\nu})}|^2$ for the antineutrino induced reaction (3) is simply obtained from eq. (4) by the crossing substitution $k_1 \leftrightarrow k_2$.

The distribution in polar angle ϑ of the hadronic energy in neutrino production is first calculated from eq. (2) in the rest system of the final hadrons, for fixed $\boldsymbol{q}$. The result is cast in Lorentz-invariant form, and the muon phase-space integration $\int d^3k_2/2k_2^0(2\pi)^3$ is performed in the laboratory frame, where $P=(M,\mathbf{0})$, $P\cdot q = M\nu$. The final result for $(i,j)=(q,q)$, in the most integrated form*, is computed from

$$\frac{d\Sigma_{qq}^{(\nu)}}{d\cos\vartheta} = \int_{Q_0^2}^{Q_M^2} dQ^2 \int_{\xi_0}^{\xi_M} \frac{d\xi}{\xi} \frac{d\tilde{\Sigma}_{qq}^{(\nu)}}{dQ^2\, d\xi\, d\cos\vartheta} f_q(\xi, Q^2),$$

$$\frac{d\tilde{\Sigma}_{qq}^{(\nu)}}{dQ^2\, d\xi\, d\cos\vartheta} = \tfrac{4}{3} K(Q^2) \frac{Q^2}{2\xi \sin^2 \tfrac{1}{2}\vartheta} \times \int_{\nu_0}^{\nu_M} d\nu \frac{(2M\nu\xi - Q^2)\sqrt{2M\nu - Q^2}\, f_1(Q^2,\xi,\nu,\vartheta)}{\nu^3 (2M\nu\vartheta_\xi - Q^2)^4},$$

$$f_1 = (2M\nu\xi - Q^2)^2 f_2(Q^2,\xi,\nu,\vartheta) + 8\left[E_1 M\nu\xi (2M\nu\vartheta_\xi - Q^2)\right]^2,$$

$$f_2 = E_1 Q^2 (E_1 - \nu)(2M\nu - Q^2)\sin^2\vartheta + 2\left[E_1 Q^2 \cos\vartheta - \nu(2M\nu - Q^2 - 2ME_1)\sin^2\tfrac{1}{2}\vartheta \right]^2,$$

$$\vartheta_\xi = \sin^2\tfrac{1}{2}\vartheta + \xi\cos^2\tfrac{1}{2}\vartheta, \qquad K(Q^2) = \frac{\alpha_s(Q^2)G^2}{32\pi^2 M^2 E_1^2}. \tag{5}$$

The integration limits,

$$\nu_0 = \frac{Q^2}{2M\xi}, \qquad \nu_M = \frac{4E_1^2 - Q^2}{4E_1},$$

$$\xi_0 = \frac{2E_1 Q^2}{M(4E_1^2 - Q^2)}, \qquad \xi_M = \frac{Q^2}{Q^2 + W_0^2},$$

$$Q_M^2 = \frac{2E_1(2ME_1 - W_0^2)}{2E_1 + M}, \qquad W \geqslant W_0,$$

* Complete integration of leptonic momenta in the final state is desirable to ameliorate the low statistics problem, expected to confront early data [14].

are essentially determined by $(p_j + p_k)^2 \geqslant 0$ and $|\cos(\hat{k}_1, \hat{k}_2)| \leqslant 1$. The lower limits Q_0, W_0 have been introduced to fulfill specific experimental requirements (cuts). The additional terms, $\mathrm{d}\Sigma^{(\nu)}_{\mathrm{qg},\ldots,\mathrm{g\bar{q}}}/\mathrm{d}\cos\vartheta$, needed in the final expression $\mathrm{d}\Sigma^{(\nu)}/\mathrm{d}\cos\vartheta$ are given in appendix A.

The useful measure $\mathrm{d}\Sigma/\mathrm{d}\cos\vartheta\,\mathrm{d}\nu$, $\nu \in [\nu_1, \nu_2]$ is also extracted from eq. (5). Simple rearrangement of the integration variables gives for the new limits, Q'^2_{M}, ξ'_0, ν_1 and ν_2 the values

$$Q'^2_{\mathrm{M}} \simeq 2M\nu - W_0, \qquad \xi'_0 = \frac{Q^2}{2M\nu},$$

$$\nu_1 = \frac{Q_0^2 + W_0^2}{2M}, \qquad \nu_2 = E_1 - \frac{Q_0^2}{4E_1},$$

with the same Q_0^2 and ξ_{M} as above.

The azimuthal correlation of hadronic energy flow with respect to the lepton plane, $\mathrm{d}\Sigma/\mathrm{d}\cos\vartheta\,\mathrm{d}\varphi$, obviously probes QCD in more detail at the expense, however, of data quality. A similar analysis to the one mentioned before eq. (5) leads to the (partial) result

$$\frac{\mathrm{d}\Sigma^{(\nu)}_{\mathrm{qq}}}{\mathrm{d}\Omega} = \int_{Q_0^2}^{Q_{\mathrm{M}}^2} \mathrm{d}Q^2 \int_{\xi_0}^{\xi_{\mathrm{M}}} \frac{\mathrm{d}\xi}{\xi} \frac{\mathrm{d}\tilde{\Sigma}^{(\nu)}_{\mathrm{qq}}}{\mathrm{d}Q^2\,\mathrm{d}\xi\,\mathrm{d}\Omega} f_{\mathrm{q}}(\xi, Q^2),$$

$$\frac{\mathrm{d}\tilde{\Sigma}^{(\nu)}_{\mathrm{qq}}}{\mathrm{d}Q^2\,\mathrm{d}\xi\,\mathrm{d}\Omega} = \tfrac{4}{3} K(Q^2) \frac{Q^2}{2\pi\xi \sin^2 \tfrac{1}{2}\vartheta}$$

$$\times \int_{\nu_0}^{\nu_{\mathrm{M}}} \mathrm{d}\nu \frac{(2M\nu\xi - Q^2)\sqrt{2M\nu - Q^2}\, F_1(Q^2, \xi, \nu, \vartheta, \varphi)}{\nu^3 \left(2M\nu\vartheta_\xi - Q^2\right)^4}, \qquad (6)$$

$$F_1 = (2M\nu\xi - Q^2) F_2^2(Q^2, \xi, \nu, \vartheta, \varphi) + 4\left[E_1 M\nu\xi\left(2M\nu\vartheta_\xi - Q^2\right)\right]^2,$$

$$F_2 = \left[Q^2 E_1 \cos\vartheta - \nu\left(2M\nu - Q^2 - 2ME_1\right)\sin^2\tfrac{1}{2}\vartheta\right]$$

$$- \left[E_1 Q^2 (E_1 - \nu)(2M\nu - Q^2)\sin^2\vartheta\right]^{1/2} \cos\varphi.$$

Similar expressions hold for the five remaining neutrino terms, while the antineutrino case is easily worked out via eq. (A.1) [see appendix A].

3. Non-perturbative background

The QCD results of sect. 2 are expected to be valid at asymptotic energies. At presently available energies, however, the non-perturbative (NP) effects may play an important role. These include parton fragmentation into hadrons (with finite

transverse momenta) which results into angular smearing of the primary distribution.

In our case the most important NP effect is the smearing of the two-jet events, that is, the zero-order contribution. The primary energy distribution to this order is proportional to a delta function centered at $\vartheta = 0, \pi$. As a result of hadronization, this delta function is smoothed out and the probability to detect a finite amount of energy at large polar angles is different from zero. The question is, how big this contribution is in comparison with the three-jet perturbation result.

In this section we estimate in a simple model this NP background in the current fragmentation region. A gaussian type of angular distribution is assumed for the hadrons in the forward jet. This leads to

$$\left(\frac{\mathrm{d}\Sigma}{\mathrm{d}\vartheta}\right)_{\mathrm{NP}} = \int_{Q_0^2}^{Q_M^2} \mathrm{d}Q^2 \int_{\nu_0'}^{\nu_M} \mathrm{d}\nu D(\vartheta, W) \frac{\mathrm{d}\Sigma_0}{\mathrm{d}Q^2\,\mathrm{d}\nu}, \tag{7}$$

where

$$D(\vartheta, W) = \frac{2\vartheta}{(\Delta\vartheta)^2} \exp\{-\vartheta^2/(\Delta\vartheta)^2\}, \qquad \nu_0' = \frac{Q^2 + W_0^2}{2M}.$$

Σ_0 is the zero-order energy cross section. The characteristic breadth $\Delta\vartheta$ is determined from the single-hadron inclusive distribution with the usual assumption about the transverse momentum dependence,

$$\frac{\mathrm{d}\sigma}{\mathrm{d}z\,\mathrm{d}h_T^2} = F(z)\,\mathrm{e}^{-4h_T^2}. \tag{8}$$

h_T is the hadron transverse momentum relative to the jet axis, and $z = 2p_h/W$, p_h the momentum of the hadron. The breadth $\Delta\vartheta$ is proportional to $\sin^{-1}(\langle\sin\vartheta\rangle)$, where $\langle\sin\vartheta\rangle = \langle h_T/p_h\rangle$ is given by

$$\frac{\langle\sin\vartheta\rangle}{\langle h_T\rangle} = \frac{\int_0^1 \mathrm{d}z \int_0^{p_h^2} \mathrm{d}h_T^2 \sin\vartheta\, \mathrm{d}\sigma^h/\mathrm{d}z\,\mathrm{d}h_T^2}{\int_0^1 \mathrm{d}z \int_0^{p_h^2} \mathrm{d}h_T^2 h_T\, \mathrm{d}\sigma^h/\mathrm{d}z\,\mathrm{d}h_T^2}. \tag{9}$$

We consider three different parametrizations for $F(z)$.

(α) The single hadron inclusive data in $\mathrm{e}^+\mathrm{e}^- \to \mathrm{h} + \mathrm{X}$ [15] is fitted by a simple exponential

$$zF(z) = \mathrm{e}^{\beta z}. \tag{10}$$

(β) $zF(z) = 0.05 + 1.05\,(1-z)^2$, (11)

which is a Field and Feynman-like fragmentation function [16].

(γ) A Q^2 dependent, QCD-inspired parametrization [17]

$$zF(z, Q^2) = c(\bar{s}) z^{d_1(\bar{s})} (1-z)^{d_2(\bar{s})}, \tag{12}$$

where

$$c(\bar{s}) = 0.50 - 0.07\bar{s},$$

$$d_1(\bar{s}) = -0.29\bar{s} + 0.06\bar{s}^2,$$

$$d_2(\bar{s}) = 1.0 + 0.59\bar{s} + 0.05\bar{s}^2,$$

$$\bar{s} = \ln\frac{\ln(Q^2/\Lambda^2)}{\ln(Q_0^2/\Lambda^2)}.$$

At large hadronic invariant mass $\Delta\vartheta$ exhibits the expected behaviour

$$\Delta\vartheta \propto \frac{\langle h_T\rangle}{W}\ln\frac{W}{\langle h_T\rangle}, \qquad W \gg \langle h_T\rangle \approx 0.3\ \text{GeV}/c.$$

4. Results

We are now going to present and discuss the results of sects. 2, 3. The polar angle distribution of hadronic energy for neutrinoproduction [eqs. (3), (5)] is shown in figs. 3a, (b) for $E_l = 200$ (1000) GeV. On each figure the scale on the left-hand

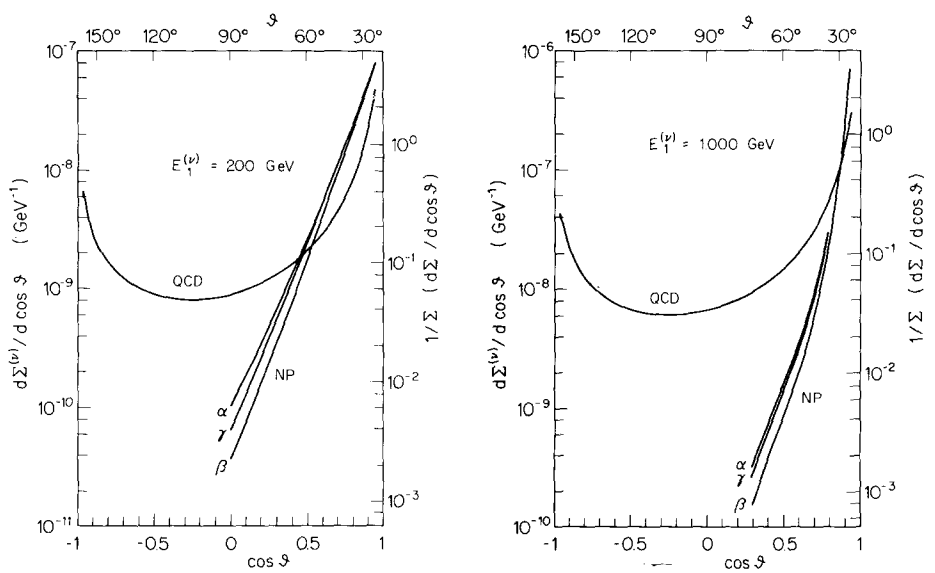

Fig. 3. a (b): QCD prediction to the first order in α_s for the hadronic "antenna pattern" in neutrino production off an isoscalar target, for beam energy $E_l = 200$ (1000) GeV. NP stands for the hadronised two-jet contribution in the current fragmentation region of fig. 2. NP (α, β, γ) represent three different parametrizations for the NP background, as discussed in sect. 3.

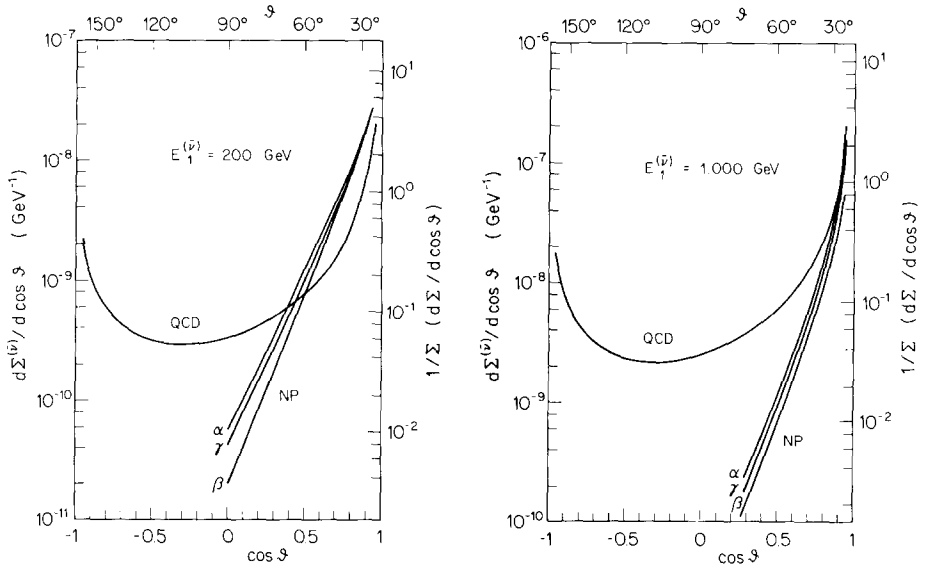

Fig. 4. Same as in fig. 3. The initial lepton is now an antineutrino.

side measures $d\Sigma^{(\nu)}/d\cos\vartheta$ in GeV^{-1} and on the other side measures the same magnitude divided by the fully integrated energy cross section Σ. We have used the "counting-rule-like" structure functions of ref. [18] with $\alpha_s = 12\pi/25\log(Q^2/\Lambda^2)$, $\Lambda = 0.5$ GeV, $Q_0^2 = 1.8$ GeV^2 and $W_0 = 2$ GeV. The variation between $W_0 = 2$ GeV and zero is not more than 2%. The same cross section for $\bar{\nu}$ is presented in figs. 4a,(b). The two distributions are very similar in shape. There is, however, an overall reduction in magnitude for $\bar{\nu}$, by a factor of ~ 3. One observes that a fivefold increase in the neutrino energy E_l augments the energy deposited around $\vartheta = 90°$ by a factor ~ 8, while the *relative* perturbative result falls by 25% in the same angular range. Obviously, the QCD "valley" in figs. 3 and 4 grows with E_l slower than Σ. As noted earlier, the perturbation expansion is not to be trusted in the vicinity of $\vartheta = 0$ where $\langle\alpha_s\rangle \log\vartheta \geqslant 1$. The same happens at $\vartheta \simeq \pi$ dominated by hadronization of the "spectator" constituents of the target, neglected here.

The NP contribution is also given in figs. 3 and 4 for the three parametrizations in eqs. (10)–(12). The simple exponential (α) stays higher than the others at large angles. Their difference here is mainly due to their different behaviour around $z = 0$. This difference becomes important at $E_l \leqslant 50$ GeV where the NP background is close to the three-jet result around 90°. For example at $E_l = 20$ GeV the QCD result can no longer be distinguished from NP(α), while NP(β) stays a factor of ~ 3 below, at $\vartheta = 90°$. At higher energies, on the other hand, all three NP(α, β, γ) curves lie well below the perturbative result, a fact shown explicitly at $E_l = 200$ and 1000 GeV. This comparison indicates that a test of QCD should be possible even at $E_l = 200$ GeV.

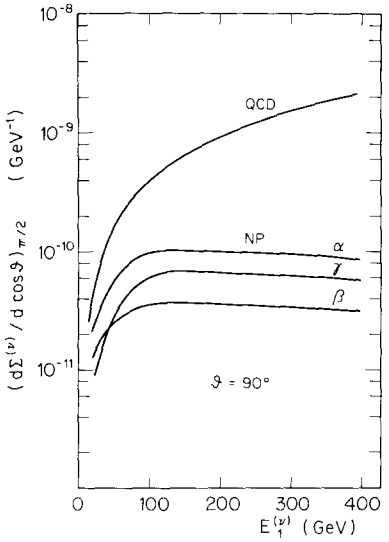

Fig. 5. Energy dependence of QCD antenna patterns for incoming neutrinos at fixed polar angle $\vartheta = 90°$. NP (α, β, γ) refers to two-jet hadronization contribution in the fragmentation region for the parametrization defined in sect. 3.

One could directly disentangle the perturbative result from the NP background through a study of their respective energy dependences. This is shown in fig. 5 for incoming neutrinos at $\vartheta = 90°$. We see that between $E_1 = 100$ GeV and 400 GeV the QCD contribution increases by a factor of six, while the NP curve stays constant or falls slightly for all parametrizations. For antineutrinos one obtains similar results. This trend should constitute a model-independent way to judge experimentally whether QCD dominates the NP background at present energies.

The question of how sensitive our result is to the specific choice of structure functions in eq. (5), is examined next. A power-type parametrization $f(\xi, Q^2) = (Q^2/Q_0^2)^{g(\xi)} f(\xi, Q_0^2)$ suggested by conventional renormalizable field theories is tested with input $f(\xi, Q_0^2)$ taken from ref. [19], and $g(\xi)$ from ref. [20], see appendix B. In figs. 6a, b we compare $d\Sigma^{(\bar{\nu})}/d\cos\vartheta$ at $E_1 = 100$ GeV for the two sets of structure functions. The contributions for initial $q, \bar{q}$ and g are given separately. The individual q, g terms are quite different, while the total $d(\Sigma_q^{(\bar{\nu})} + \Sigma_{\bar{q}}^{(\bar{\nu})} + \Sigma_g^{(\bar{\nu})})/d\cos\vartheta$ varies only by $\sim 20\%$, because the q-term which is the dominant one remains essentially the same. It is worthwhile to relate also that the $d\Sigma^{(\nu)}/d\cos\vartheta$ result is even less sensitive to the specific choice of distribution functions. The corresponding variation is only about 4% at $E_1 = 100$ GeV*.

The antenna patterns considered so far in this paper are defined on the two-dimensional parametric space $(E_1, \cos\vartheta)$. In what follows we examine the

* This difference being so slight and not visible in our scale, we have shown the figures for the corresponding antineutrino (5a, b).

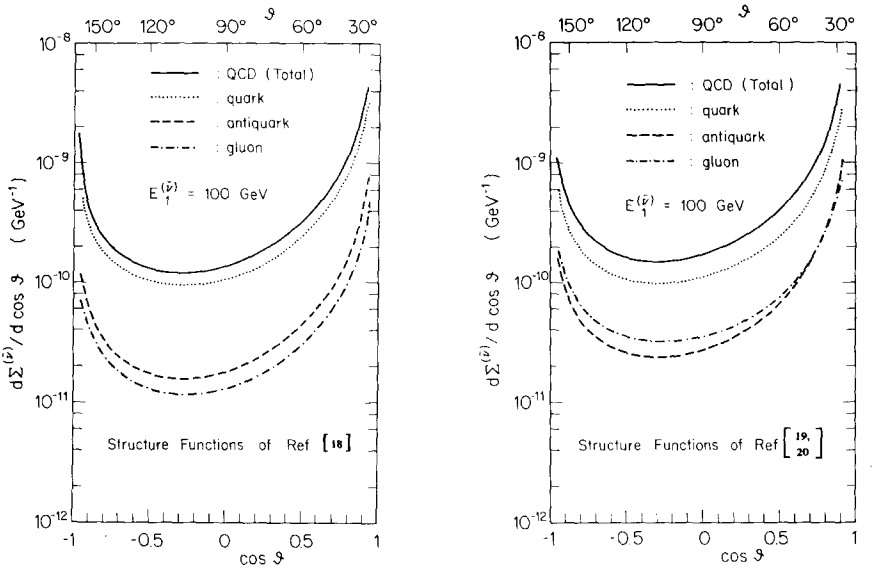

Fig. 6. Comparison of QCD antineutrino results for two different sets of structure functions (see appendix B): (a) structure functions of ref. [18]; (b) structure functions of refs. [19, 20]. The contributions of initial partons; quark, antiquark, gluon, are given separately.

same distributions in a kinematic domain augmented by one variable (Q^2 or ν). A richer structure is naturally revealed at the expense, however, of lower statistics measurements. Similar observables defined on even higher dimensional kinematic manifolds have been studied in refs. [12, 21]. Fig. 7 shows the Q^2 dependence of the energy flow perpendicular to the current direction when hadronic production is initiated at 200 GeV incident energy*. Although at middle-range Q^2 values the three-jet result seems rather well separated from the NP one, the situation is not so clear at higher/lower Q^2 values. A more useful quantity in that respect, $(d\Sigma/d\cos\vartheta\, d\nu)$ at $\vartheta = 90°$, is plotted in figs. 8a, b for ν, $\bar{\nu}$ respectively, at $E_1 = 200$ GeV. It is evident that QCD and NP backgrounds exhibit a quite different behaviour in energy transfer ν and could easily be separated above ~ 50 GeV.

We investigate finally the azimuthal energy correlation $(d\Sigma/d\cos\vartheta\, d\varphi)$ at $\vartheta = \frac{1}{2}\pi$. The result is depicted in fig. 9a along with the constant** NP background for neutrino-produced hadrons at $E_1 = 100$ GeV. The smooth variation in φ is attributed to the fact that from the two terms in the leading qq amplitude, eq. (4), the φ-independent one, $\propto (k_1, p_1)$, dominates the other. The hadronic energy is

* From now on, only the simple exponential parametrization (α) for the NP background is presented. The other two (β, γ) lie slightly below (α) and exhibit similar behaviour.

** The NP background due to primordial transverse momentum, which is neglected here, is expected to give a non-trivial φ-dependence. [22].

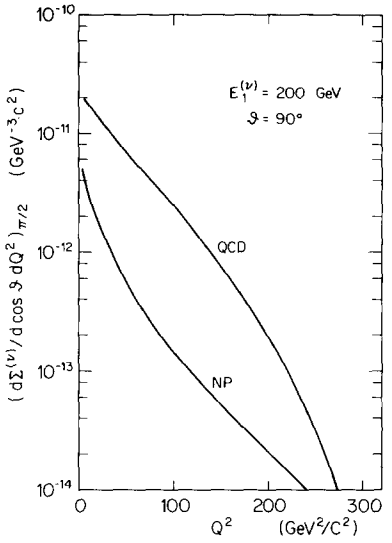

Fig. 7. Q^2 dependence of hadronic energy flow transverse to the current direction.

preferentially emitted along the lepton plane, towards the beam direction. As shown in fig. 9b, where only the leading contribution of the initial quark is considered, it is gluon-jet dominance at $\vartheta = \frac{1}{2}\pi$ which enforces the azimuthal asymmetry. This is in agreement with existing $\langle \varphi \rangle$ estimates [23].

One may repeat, in conclusion, the main thesis of this work. QCD seems to be testable in leptoproduction processes at present energies, provided an appropriate

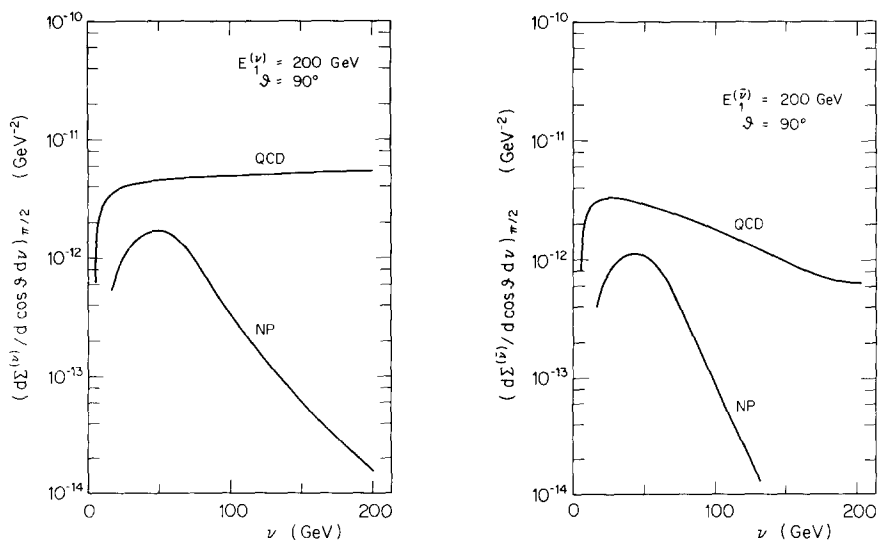

Fig. 8. a (b): ν-dependence of hadronic energy flow transverse to the current direction for initial neutrino (antineutrino).

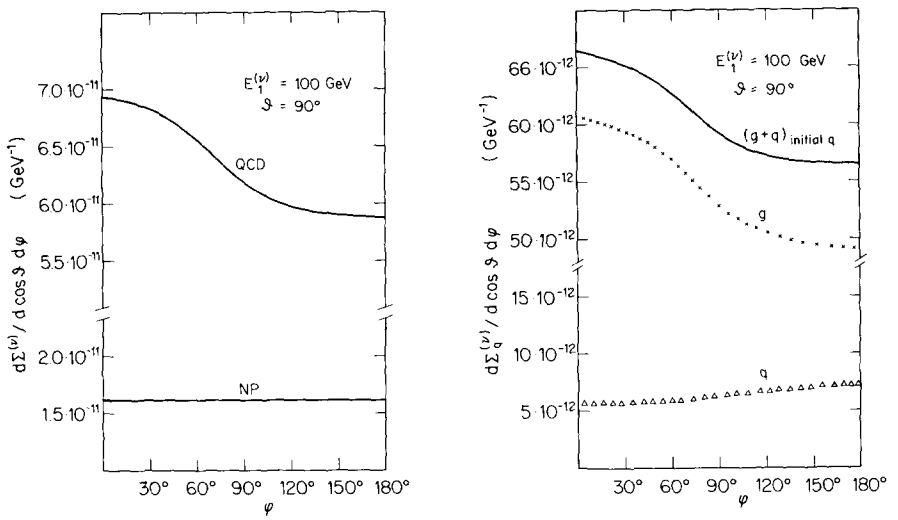

Fig. 9. (a) Azimuthal correlation of hadronic energy flow transverse to the current direction. (b) As in (a), for the infrared-finite part of quark initiated hadroproduction. The quark-jet and gluon-jet contributions are shown separately.

observable like angular flow of hadronic energy is tried. Specially, the perturbative neutrino result at $E_1 \gtrsim 200$ GeV

shows remarkable stability with respect to structure function uncertainties;

stays well above the NP estimate at large polar angles;

exhibits a quite different ν-dependence at $\vartheta \simeq \frac{1}{2}\pi$ in comparison with the non-perturbative background. Therefore a plot of $\mathrm{d}\Sigma/\mathrm{d}\cos\vartheta\,\mathrm{d}\nu$ versus ν as in fig. 8a with Λ in $\alpha_s(Q^2)$ left free to be fixed by experiment, should also afford another realistic possibility to measure the fundamental length of QCD, in deep inelastic scattering.

Appendix A

Massless kinematics simplifies the calculation through the relations ($i = \mathrm{q}, \mathrm{g}$)

$$\sum' |T_i^{(\nu,\bar{\nu})}(k_1,k_2)|^2 = \sum' |T_i^{(\nu,\bar{\nu})}(k_2,k_1)|^2,$$

$$\sum' |T_i^{(\nu,\bar{\nu})}(k_1,k_2)|^2 = \sum' |T_i^{(\bar{\nu},\nu)}(k_2,k_1)|^2, \tag{A.1}$$

which are proved by inspection in eq. (4) and crossing in the lepton vertex, respectively.

The polar distribution of hadronic energy, $d\Sigma/d\cos\vartheta$, consists of six components in first-order perturbation theory [see eq. (2)]:

$$\frac{d\Sigma}{d\cos\vartheta} = \int dQ^2 \frac{d\xi}{\xi} \left\{ f_q \frac{d\left[\tilde{\Sigma}_{qq} + \tilde{\Sigma}_{qg}\right]}{dQ^2\, d\xi\, d\cos\vartheta} + f_{\bar{q}} \frac{d\left[\tilde{\Sigma}_{\bar{q}\bar{q}} + \tilde{\Sigma}_{\bar{q}g}\right]}{dQ^2\, d\xi\, d\cos\vartheta} + f_g \frac{d\left[\tilde{\Sigma}_{gq} + \tilde{\Sigma}_{g\bar{q}}\right]}{dQ^2\, d\xi\, d\cos\vartheta} \right\} \tag{A.2}$$

with the same limits of integration as in eq. (5). The first equation of (A.1) permits the following compact presentation in terms of the Bjorken variable $x = Q^2/2P\cdot q$:

$$\frac{d\tilde{\Sigma}^{(\nu)}_{qq,\bar{q}\bar{q}}}{dQ^2\, d\xi\, d\cos\vartheta} = \tfrac{4}{3} K(Q^2) \frac{\sqrt{Q^2}}{\xi \sin^2 \tfrac{1}{2}\vartheta} \int_{\xi_0}^{\xi} \frac{dx}{\sqrt{x}} \frac{(\xi - x)\sqrt{1-x}}{(\vartheta_\xi - x)^4} \left\{ L_{1,2}^2 + M_{1,2}^2 + N_{2,1} \right\},$$

$$\frac{d\tilde{\Sigma}^{(\nu)}_{qg,\bar{q}g}}{dQ^2\, d\xi\, d\cos\vartheta} = \tfrac{4}{3} K(Q^2) \frac{\sqrt{Q^2}}{\xi \cos^2 \tfrac{1}{2}\vartheta} \int_{\xi_0}^{\xi} \frac{dx}{\sqrt{x}} \frac{(1-x)^{3/2}}{(\vartheta_\xi - x)^4} \left\{ L_{1,2}^2 + H_{2,1}^2 + N_{2,1} \right\},$$

$$\frac{d\tilde{\Sigma}^{(\nu)}_{gq,g\bar{q}}}{dQ^2\, d\xi\, d\cos\vartheta} = \tfrac{4}{8} K(Q^2) \frac{\sqrt{Q^2}}{\xi^2 \sin^2 \tfrac{1}{2}\vartheta \cos^2 \tfrac{1}{2}\vartheta} \int_{\xi_0}^{\xi} \frac{dx}{\sqrt{x}} \frac{(\xi - x)\sqrt{1-x}}{(\vartheta_\xi - x)^3}$$

$$\times \left\{ M_{2,1}^2 + H_{1,2}^2 + N_1 + N_2 \right\}, \tag{A.3}$$

where $K(Q^2)$, ϑ_ξ and ξ_0 are defined in eq. (5). The functions L, M, N and H are given by

$$L_{1,2} = 2M\xi(\vartheta_\xi - x)E_{1,2},$$

$$M_{1,2} = (\xi - x)\left[(1 - z + 2zx)ME_{1,2} - (1-z)Q^2\sigma_{1,2}\right],$$

$$N_{1,2} = 2M \sin^2\vartheta E_{1,2}(1-x)(\xi - x)^2\left(ME_{1,2}x - \sigma_{1,2}Q^2\right),$$

$$H_{1,2} = M_{1,2} - 2(\vartheta_\xi - x)\left(ME_{1,2}\xi - \sigma_{1,2}Q^2\right),$$

where

$$E_2 = E_1 - \nu = E_1 - \frac{Q^2}{2Mx}, \qquad \sigma_{1,2} = \pm\tfrac{1}{2}, \qquad z = \cos\vartheta. \tag{A.4}$$

One can easily verify that the first equation of (A.3) contains eq. (5) for $x = Q^2/2Mv$. The same connection pertains between eq. (6) and the double expression

$$\frac{\mathrm{d}\tilde{\Sigma}^{(\nu)}_{\mathrm{qq},\bar{\mathrm{q}}\bar{\mathrm{q}}}}{\mathrm{d}Q^2\,\mathrm{d}\xi\,\mathrm{d}\Omega} = \tfrac{4}{3}K(Q^2)\frac{\sqrt{Q^2}}{2\pi\xi\sin^2\frac{1}{2}\vartheta}\int_{\xi_0}^{\xi}\frac{\mathrm{d}x}{\sqrt{x}}\frac{(\xi-x)\sqrt{1-x}}{(\vartheta_\xi - x)^4}$$

$$\times\left\{L^2_{1,2} + \left[M_{2,1} - \cos\varphi\sin\vartheta\sqrt{h_{2,1}}\,\right]^2\right\},$$

where

$$h_{1,2} = 2ME_{1,2}(1-x)(\xi-x)M_{1,2}|_{z=1}. \tag{A.5}$$

The antineutrino distributions are given by (A.3) and (A.5) using $\mathrm{d}\tilde{\Sigma}^{(\bar{\nu})}_{\mathrm{if}} = \mathrm{d}\tilde{\Sigma}^{(\nu)}_{\bar{\mathrm{i}}\bar{\mathrm{f}}}$, which is another consequence of (A.1).

Appendix B

PARAMETRIZATIONS OF THE STRUCTURE FUNCTIONS

(i) All our results have been calculated with the help of structure functions taken from Owens and Reya [18].

In the usual notation we have:

$$u = u_{\mathrm{v}} + S, \qquad d = d_{\mathrm{v}} + S,$$

where $S = \bar{u} = \bar{d} = s = \bar{s}$ is the sea contribution.

$$\xi u_{\mathrm{v}}(\xi, Q^2) + \xi d_{\mathrm{v}}(\xi, Q^2) = \frac{\xi}{B(\eta_1, 1+\eta_2)}\xi^{\eta_1}(1-\xi)^{\eta_2},$$

$$\xi d_{\mathrm{v}}(\xi, Q^2) = \frac{1}{B(\eta_3, 1+\eta_4)}\xi^{\eta_3}(1-\xi)^{\eta_4},$$

with

$$\eta_1 = 0.7 - 0.176\bar{s}, \qquad \eta_2 = 2.6 + 0.8\bar{s},$$

$$\eta_3 = 0.85 - 0.24\bar{s}, \qquad \eta_4 = 3.35 + 0.816\bar{s},$$

where

$$\bar{s} = \ln\left[\ln(Q^2/\Lambda^2)/\ln(Q^2/\Lambda^2)\right], \qquad Q_0^2 = 1.8\ \mathrm{GeV}^2, \qquad \Lambda \simeq 0.5.$$

The sea S and gluon G contributions are given by

$$\xi S(\xi, Q^2) = A_s(1-\xi)^{\eta_s} + A'_s(1-\xi)^{\eta'_s} + B_s\, e^{-C_s\xi},$$

$$\xi G(\xi, Q^2) = A_g(1-\xi)^{\eta_g} + A'_g(1-\xi)^{\eta'_g} + B_g\, e^{-C_g\xi},$$

with

$$A_s \simeq 0.15 - 0.12\bar{s} + 0.03\bar{s}^2, \qquad A_g \simeq 2.41 - 1.98\bar{s} + 0.44\bar{s}^2,$$

$$A'_s \simeq 0.185\bar{s} - 0.061\bar{s}^2, \qquad A'_g \simeq 3.6\bar{s} - 1.41\bar{s}^2,$$

$$\eta_s \simeq 7.0 + 0.022\bar{s} + 0.004\bar{s}^2, \qquad \eta_g \simeq 5.0 + 1.55\bar{s} - 0.529\bar{s}^2,$$

$$\eta'_s \simeq 9.5 + 1.017\bar{s} - 0.105\bar{s}^2, \qquad \eta'_g \simeq 13.8 + 0.79\bar{s} - 0.28\bar{s}^2,$$

$$B_s \simeq 0.169\bar{s} + 0.447\bar{s}^2, \qquad B_g \simeq 7.66\bar{s} - 1.46\bar{s}^2,$$

$$C_s \simeq 25.89 + 3.96\bar{s} + 1.63\bar{s}^2, \qquad C_g \simeq 36.79 + 12.59\bar{s} - 1.16\bar{s}^2.$$

(ii) A second parametrization for the structure functions is chosen in order to compare the two different results:

$$f_i(\xi, Q^2) = \left(\frac{Q^2}{Q_0^2}\right)^{g(\xi)} f_i(\xi, Q_0^2),$$

$$g(\xi) = 0.213 - 0.98\xi + \frac{5.9\cdot 10^{-4}}{\xi}.$$

The $f_i(\xi, Q_0^2)$ are taken from Fox [19] and the $g(\xi)$ from Karlinger and Sullivan [20].

In the usual notation we have:

$$\xi u = \tfrac{1}{4}(1-\xi)^8 + \xi(1-\xi)^3(b_0 + b_1T_1 + b_2T_2 + b_3T_3) + \xi^{1/2}(1-\xi)^3(30 + 27T_1),$$

$$\xi d = \tfrac{1}{4}(1-\xi)^7 + \xi(1-\xi)^4(d_0 + d_1T_1 + d_2T_2 + d_3T_3) + \xi^{1/2}(1-\xi)^4(4.1 + 3.8T_1),$$

$$\xi S = \tfrac{1}{8}\left[(1-\xi)^7 + (1-\xi)^8\right],$$

$$\xi G = (6.35 + 5.48T_1)(1-\xi)^5,$$

where T_l are Chebyshev polynominals

$$T_l = T_l(2\xi - 1),$$

$$T_1(x) = x,$$

$$T_2(x) = 2x^2 - 1,$$

$$T_3(x) = 4x^3 - 3x,$$

and

$$b_0 = -35.37, \quad b_1 = -19.34, \quad b_2 = 1.54, \quad b_3 = 0.73,$$

$$d_0 = -3.1, \quad d_1 = 6.76, \quad d_2 = -0.86, \quad d_3 = -1.60.$$

References

[1] M.K. Gaillard, LAPP-TH-03, Rapporteur talk at the European Physical Society Int. Conf. on High-energy physics, Geneva (1979)
[2] G. Sternman and S. Weinberg, Phys. Rev. Lett. 39 (1977) 1436
[3] H. Georgi and M. Machachek, Phys. Rev. Lett. 39 (1977) 1237
[4] E. Fahri, Phys. Rev. Lett. 39 (1977) 1587
[5] A. De Rújula, J. Ellis, E.G. Floratos and M.K. Gaillard, Nucl. Phys. B138 (1978) 387
[6] C.L. Basham, L.S. Brown, S.D. Ellis and S.T. Love, Phys. Rev. Lett. 41 (1978) 1858; Phys. Rev. D17 (1978) 2298;
L.S. Brown, Seattle preprint PLO-1388 (1977)
[7] G. Tiktopoulos, Nucl. Phys. B147 (1979) 371
[8] I.I.Y. Bigi and T.F. Walsh, Phys. Lett. 82B (1979) 267;
I.I.Y. Bigi, Phys. Lett. 79B (1978) 262; CERN preprint TH-2626 (1979)
[9] H. Georgi and H.D. Politzer, Phys. Rev. Lett. 40 (1978) 3
[10] G. Sternman, Phys. Rev. D17 (1978) 2789
[11] P. Binétruy and G. Girardi, Nucl. Phys. B155 (1979) 150
[12] R.D. Peccei and R. Rückl, Phys. Lett. 84B (1979) 95; Nucl. Phys. B162 (1980) 125
[13] E. Manesis and N.A. Papadopoulos, Phys. Lett. 86B (1979) 361
[14] K. Winter, private communication
[15] C.G. Hanson, Tbilisi Conf. 1976, SLAC-PUB1814 (1976);
R. Brandelik et al., DASP-Collaboration, Phys. Lett. 67B (1977) 358
[16] R.D. Field and R.P. Feynman, Phys. Rev. D15 (1977) 2590;
L.M. Sehgal, Proc. 1977 Int. Symp., Hamburg
[17] R. Baier, J. Engels and B. Peterson, BI-TP79/10 (1979)
[18] J.F. Owens and E. Reya, Phys. Rev. D17 (1978) 3003
[19] G.C. Fox, Nucl. Phys. B131 (1977) 107
[20] I. Karlinger and J.D. Sullivan, University of Illinois preprint ILL-(TH)-78-20
[21] M. Kuroda, Bielefeld preprint, BI-TP-79/20
[22] R. Cahn, Phys. Lett. 78B (1978) 269
[23] H. Georgi and H.D. Politzer, Phys. Rev. Lett. 40 (1978) 3;
J. Cleymans, Phys. Rev. D18 (1978) 954